Nocturnal Atmospheric Synergistic Oxidation Reduces the Formation of Low-volatility Organic Compounds from Biogenic Emissions

Han Zang[1], Zekun Luo[1], Chenxi Li[1], Ziyue Li[1], Dandan Huang[2,*], Yue Zhao[1,*]

[1]School of Environmental Science and Engineering, Shanghai Jiao Tong University, Shanghai, 200240, China

[2]Shanghai Academy of Environmental Sciences, Shanghai, 200233, China

*Correspondence: Yue Zhao (yuezhao20@sjtu.edu.cn); Dandan Huang (huangdd@saes.sh.cn);

Abstract

Volatile organic compounds (VOCs) are often subject to synergistic oxidation by different oxidants in the atmosphere. However, the exact synergistic oxidation mechanism of atmospheric VOCs and its role in particle formation remain poorly understood. In particular, the reaction kinetics of the key reactive intermediates, organic peroxy radicals (RO_2), during synergistic oxidation is rarely studied. Here, we conducted a combined experimental and kinetic modelling study of the nocturnal synergistic oxidation of α-pinene (the most abundant monoterpene) by O_3 and NO_3 radicals as well as its influences on the formation of highly oxygenated organic molecules (HOMs) and particles. We find that in the synergistic O_3 + NO_3 regime, where OH radicals are abundantly formed via decomposition of ozonolysis-derived Criegee intermediates, the production of $C_xH_yO_z$-HOMs is substantially suppressed compared to that in the O_3-only regime, mainly because of the depletion of of α-pinene RO_2 derived from ozonolysis and OH oxidation by those arising from NO_3 oxidation via cross reactions. Measurement-model comparisons further reveal that the cross-reaction rate constants of NO_3-derived RO_2 with O_3-derived RO_2 are on average 10 – 100 times larger than those of NO_3-derived RO_2 with OH-derived RO_2. Despite a strong production of organic nitrates in the synergistic oxidation regime, the substantial decrease of $C_xH_yO_z$-HOM formation leads to a significant reduction in ultralow- and extremely low-volatility organic compounds, which significantly inhibits the formation of new particles. This work provides valuable mechanistic and quantitative insights into the nocturnal synergistic oxidation chemistry of biogenic emissions and will help to better understand the formation of low-volatility organic compounds and particles in the atmosphere.

1. Introduction

The Earth's atmosphere is a complex oxidizing environment in which multiple oxidants coexist. During the nighttime, NO_3 radicals (generated by the reaction of NO_2 and O_3) and O_3 contribute significantly to the oxidation of volatile organic compounds (VOCs) (Huang et al., 2019), while during the daytime, the fast photolysis of NO_3 radicals and rapid photochemical formation of OH radicals and O_3 make the latter two the major oxidants for VOCs (Zhang et al., 2018). Therefore, the degradation of ambient VOCs is subject to concurrent oxidation by different oxidants. Gas-phase oxidation of VOCs from biogenic emissions (BVOCs) by these major atmospheric oxidants produces a key type of reactive intermediates, organic peroxy radicals (RO_2), a portion of which can undergo fast autoxidation forming a class of highly oxygenated organic molecules (HOMs) with low volatilities (Jokinen et al., 2014; Mentel et al., 2015; Berndt et al., 2016; Zhao et al., 2018; Iyer et al., 2021; Shen et al., 2022; Ehn et al., 2014). HOMs typically contain six or more oxygen atoms, and play a key role in the formation of atmospheric new particles and secondary organic aerosol (SOA) (Kirkby et al., 2016; Berndt et al., 2018; Zhao et al., 2018; Ehn et al., 2014; Bianchi et al., 2019), which have important influences on air quality (Huang et al., 2014), public health (Pye et al., 2021), and Earth's radiative forcing (Shrivastava et al., 2017).

Due to the complexity of oxidation mechanisms of BVOCs, previous laboratory studies typically featured only one oxidant and a single SOA precursor (Berndt et al., 2016; Berndt, 2021; Claflin et al., 2018; Iyer et al., 2021; Boyd et al., 2015). However, the synergistic oxidation by different oxidants may significantly alter the fate of RO_2 intermediates, therefore influencing the formation of HOMs and SOA (Bates et al., 2022). Recently, a field study at a boreal forest site in Finland observed a series of nitrate-containing HOM-dimers from the coupled O_3 and NO_3 oxidation of monoterpenes (Zhang et al., 2020). At the same site, Lee et al. (2020) found that the synergistic oxidation of BVOCs by OH radicals and O_3 contributed to the largest fraction of SOA. These studies suggest that the synergistic oxidation of BVOCs by different oxidants plays an important role in the formation of HOMs and SOA in the atmosphere and highlight the needs to investigate the synergistic oxidation mechanisms of BVOCs for a better representation of atmospheric particle formation.

Several laboratory studies have attempted to address the role of synergistic oxidation of BVOCs in the formation of new particles and SOA (Kenseth et al., 2018; Inomata, 2021; Liu et al., 2022; Li et

al., 2024). Kenseth et al. (2018) identified a suite of dimer esters in flow tube experiments that can be only formed from the OH and O_3 synergistic oxidation of β-pinene. These dimers exhibit extremely low volatility and contributed 5.9 – 25.4% to the total β-pinene SOA. Similarly, Inomata (2021) found that the presence of OH radicals during α-pinene ozonolysis is a key factor for the production of low-volatility organic species and significantly promotes new particle formation (NPF). On the other hand, the addition of O_3 in the monoterpene photooxidation system also significantly increases the SOA mass yield (Liu et al., 2022). In addition, a recent chamber study by Bates et al. (2022) showed that the synergistic oxidation of α-pinene by NO_3 radicals and O_3 can significantly enhance the SOA yield compared to the NO_3 + α-pinene regime, which has nearly 0% SOA yield (Fry et al., 2014; Hallquist et al., 1999; Mutzel et al., 2021), and they revealed that the SOA yield in the NO_3 + O_3 oxidation system largely depends on the RO_2 fates. Most recently, Li et al. (2024) found that during α-pinene ozonolysis, the presence of nitrooxy-RO_2 radicals formed from NO_3 oxidation can significantly suppress the production of ultralow-volatility organic compounds (ULVOCs) and thereby NPF. These laboratory studies together provide growing evidence that synergistic oxidation of BVOCs by different oxidants have profound impacts on atmospheric particle formation. However, the specific synergistic mechanisms of different oxidants and oxidation pathways remain obscure. Although a few studies underscored the importance of the RO_2 fates (Bates et al., 2022; Li et al., 2024), the exact interactions between RO_2 species derived from different oxidants are still unclear, and quantitative constraints on the reaction rate of different RO_2 species are quite limited.

Here we conducted an investigation of the synergistic O_3 + NO_3 oxidation of α-pinene, one of the most abundant monoterpenes in the atmosphere, using a combination of laboratory experiments and detailed kinetic modelling, and focusing on the fate of RO_2 intermediates arising from different oxidation pathways. The α-pinene oxidation experiments were conducted in a custom-built flow reactor. The molecular composition of RO_2 species and HOMs in different oxidation regimes was characterized using a chemical ionization atmospheric pressure interface time-of-flight mass spectrometer (CI-APi-ToF) employing a nitrate ion source. The measured distributions of specific RO_2 and HOMs across different oxidation regimes were fitted with a kinetic model using Master Chemical Mechanisms (MCM v3.3.1) updated with recent advances of α-pinene RO_2 chemistry

(Wang et al., 2021; Iyer et al., 2021; Shen et al., 2022; Zang et al., 2023), which allows for quantitative constraints on RO_2 kinetics and synergistic oxidation mechanisms. Atmospheric relevance of the experimental results was evaluated by modelling the investigated oxidation chemistry under typical nocturnal atmospheric conditions.

2. Materials and Methods

2.1 Flow tube experiments

Experiments of α-pinene oxidation in different regimes (i.e., synergistic O_3 + NO_3 oxidation vs. O_3-only) were carried out under room temperature (298 K) and dry (relative humidity < 5%) conditions in a custom-built flow tube reactor (FTR, Figure S1). O_3 and NO_2 were added into a glass tube (Figure S1) to form NO_3 radical and its precursor N_2O_5:

$NO_2 + O_3 \rightarrow NO_3 + O_2$ （R1）

$NO_3 + NO_2 \leftrightarrow N_2O_5$ （R2）

O_3 was generated by passing a flow of ultra-high-purity (UHP) O_2 (Shanghai Maytor Special Gas Co., Ltd.) through a quartz tube housing a pen-ray mercury lamp (UV-S2, UVP Inc.) and its concentration was measured by an ozone analyzer (T400, API). NO_2 was obtained from a gas cylinder (15.6 ppm, Shanghai Weichuang Standard Gas Co., Ltd.). The initial NO_2 concentration in the flow tube was 4.5 – 6.4 ppb. To prevent the titration of NO_3 radicals by NO, all the experiments were performed without the addition of NO. The total air flow in the NO_3 generation glass tube was 0.6 L min^{-1} and 0.4 L min^{-1} for the gas-phase HOM and SOA formation experiments, respectively. The produced N_2O_5 and NO_3 radicals, as well as the excessive O_3 were added into the FTR to initiate α-pinene oxidation. For the O_3-only experiments, only O_3 was added into FTR.

The α-pinene gas was generated by evaporating a defined volume of its liquid (99%, Sigma-Aldrich) into a cleaned and evacuated canister (SilcoCan, RESTEK), and then added into FTR through a movable injector at a flow rate of 22 – 108 mL min^{-1}. The initial concentration of α-pinene in the flow reactor ranged from 100 – 500 ppb. In some experiments, the gas of cyclohexane (~ 100 ppm), which was generated by bubbling a gentle flow of UHP N_2 through its liquid (LC-MS grade, CNW), was added into the flow reactor as a scavenger of OH radicals formed from α-pinene ozonolysis.

For experiments characterizing the formation of HOMs, the total air flow in the FTR was 10.8 L

118 min^{-1} and the residence time was 25 seconds. The short reaction time and the small amount of
119 reacted α-pinene (see Table S1) in these experiments prevented the formation of particles. For the
120 experiments characterizing the formation of SOA particles, a larger FTR was used, with a total air
121 flow of 5 L min^{-1} and a residence time of 180 seconds. A summary of the conditions including the
122 simulated concentrations of NO_2, N_2O_5 and NO_3 radicals, as well as the concentration of α-pinene
123 oxidized by each oxidant in different experiments are shown in Table S1.

124 The gas-phase RO_2 radicals and closed-shell products were measured using a nitrate-based CI-APi-
125 ToF (abbreviated as nitrate-CIMS; Aerodyne Research, Inc.), which has been described in detail
126 previously (Zang et al., 2023). A long ToF-MS with a mass resolution of ~10000 Th/Th was used
127 here. The mass spectra within the m/z range of 50 – 700 were analyzed using the tofTools package
128 developed by Junninen et al. (2010) based on Matlab. The total ion counts (TIC) with values of (5.9
129 – 6.2) $\times 10^4$ cps are similar under different reaction conditions. In this study, we assume that the
130 $C_xH_yO_z$-HOMs derived from ozonolysis and OH oxidation of α-pinene exhibit the same sensitivity
131 in nitrate-CIMS. However, the highly oxygenated organic nitrates (ONs) may have a significantly
132 lower sensitivity compared to the $C_xH_yO_z$-HOM counterparts, given that the substitution of -OOH
133 or -OH groups by $–ONO_2$ group in the molecule would reduce the number of H-bond donors, which
134 is a key factor determining the sensitivity of nitrate-CIMS (Shen et al., 2022; Hyttinen et al., 2015).
135 Recently, Li et al. (2024) used CI-Orbitrap with ammonium or nitrate reagent ions to detect
136 oxygenated organic molecules in the synergistic O_3 + NO_3 regime and found that both the ion
137 intensity of ONs and their signal contribution to the total dimers were much lower when using nitrate
138 as reagent ions.

139 A scanning mobility particle sizer (SMPS, TSI), consisting of an electrostatic classifier (model
140 3082), a condensation particle counter (model 3756), and a long or nano differential mobility
141 analyzer (model 3081 and 3085) with a measurable size range of 4.6 – 156.8 nm or 14.6 – 661.2
142 nm, respectively, was employed to monitor the formation of particles in the flow tube. During the
143 HOM formation experiments, even under conditions with the highest initial α-pinene concentration
144 (500 ppb), only a tiny amount of particles was formed, with mass concentrations of $(6.4 \pm 1.7) \times 10^{-3}$
145 and $(1.0 \pm 0.4) \times 10^{-2}$ μg m^{-3} and number concentrations of 574 ± 148 and 256 ± 68 cm^{-3} in the O_3-
146 only (Exp 5) and O_3 + NO_3 regimes (Exp 11), respectively. These results suggest that the formation

of SOA particles in the HOM formation experiments is negligible and would have no significant influence on the fate of RO_2 and closed-shell products.

2.2 Estimation of HOM volatility

A modified composition-activity method was used to estimate the saturation mass concentration (C^*) of HOMs in this study according to the approach developed by Li et al. (2016):

$$\log_{10}C^* = (n_C^0 - n_C)b_C - n_O b_O - 2\frac{n_C n_O}{n_C + n_O}b_{CO} - n_N b_N - n_S b_S$$

where n_C^0 is the reference carbon number; n_C, n_O, n_N, and n_S are the atom numbers of carbon, oxygen, nitrogen, and sulfur, respectively; b_C, b_O, b_N, and b_S are the contribution of each atom to $\log_{10}C^*$, respectively; b_{CO} is the carbon–oxygen nonideality (Donahue et al., 2011). These *b*-values were provided by Li et al. (2016).

It should be noted that the CHON compounds used in the data set by Li et al. (2016) are mostly amines, amides, and amino acids, and only contain a limited number of ONs (0.07%). Since different types of CHON compounds have very different vapor pressures (Isaacman-Vanwertz and Aumont, 2021), this formula-based approach can be biased to estimate the C^* of ONs. Considering that the $-ONO_2$ and –OH groups have similar impacts on vapor pressure and that the CHON species are predominantly ONs in our study, all $-ONO_2$ groups are treated as –OH groups during the estimation of vapor pressure (Daumit et al., 2013; Isaacman-Vanwertz and Aumont, 2021).

Gas-phase HOMs are grouped into five classes based on their $\log_{10}C^*$ (Donahue et al., 2012; Bianchi et al., 2019; Schervish and Donahue, 2020), that is, ULVOCs ($\log_{10}C^* < -8.5$), extremely low-volatility organic compounds (ELVOCs, $-8.5 < \log_{10}C^* < -4.5$), low-volatility organic compounds (LVOCs, $-4.5 < \log_{10}C^* < -0.5$), semi-volatile organic compounds (SVOCs, $-0.5 < \log_{10}C^* < 2.5$), and intermediate-volatility organic compounds (IVOCs, $2.5 < \log_{10}C^* < 6.5$).

2.3 Kinetic model simulations

Model simulations of specific RO_2 radicals and closed-shell HOMs formed in different oxidation regimes were performed to constrain the reaction kinetics and mechanisms using the Framework for 0-D Atmospheric Modeling (F0AM v4.1) (Wolfe et al., 2016), which employs MCM v3.3.1 (Jenkin et al., 2015). The α-pinene oxidation mechanism was updated with the state-of-the-art

knowledge on the chemistry of RO_2 autoxidation and cross reactions forming HOM monomers and dimers, respectively (Zhao et al., 2018; Wang et al., 2021; Iyer et al., 2021; Shen et al., 2022). The detailed updates have been described in our previous study (Zang et al., 2023). In particular, the formation and subsequent reactions of the ring-opened primary $C_{10}H_{15}O_4$-RO_2, the highly oxygenated acyl RO_2, as well as the $C_{10}H_{15}O_2$-RO_2 arising from H-abstraction by OH radicals during α-pinene ozonolysis are included in the model according to recent studies (Iyer et al., 2021; Zhao et al., 2022; Zang et al., 2023; Shen et al., 2022).

To investigate the synergistic reactions of RO_2 derived from the oxidation of α-pinene by different oxidants, we added the cross reactions of the primary nitrooxy-RO_2 derived from NO_3 oxidation ($^{NO3}RO_2$), i.e., $C_{10}H_{16}NO_5$-RO_2, with RO_2 derived from ozonolysis ($^{CI}RO_2$) and OH oxidation ($^{OH}RO_2$). Recently, Zhao et al. (2018) revealed the bulk rate constant for $^{CI}RO_2$ and $^{OH}RO_2$ self/cross reactions to be 2×10^{-12} cm^3 molecule^{-1} s^{-1}, and Bates et al. (2022) constrained the rate constant for $^{NO3}RO_2$ self/cross reactions to be $1 \times 10^{-13} - 1 \times 10^{-12}$ cm^3 molecule^{-1} s^{-1}. In the present study, the default rate constant for $^{NO3}RO_2 + {}^{CI}RO_2$ was set to 2×10^{-12} cm^3 molecule^{-1} s^{-1}, the same to that for self/cross reactions of $^{CI}RO_2$ and $^{OH}RO_2$. The default rate constant for $^{NO3}RO_2 + {}^{NO3}RO_2$ was set to 1×10^{-12} cm^3 molecule^{-1} s^{-1}. The ratio of the cross-reaction rate constant of $^{NO3}RO_2 + {}^{CI}RO_2$ to that of $^{NO3}RO_2 + {}^{OH}RO_2$ was tuned to achieve a good measurement-model agreement for the distribution of specific RO_2 and HOMs across different oxidation regimes. Recent studies suggested that the ROOR' dimer formation rates from the highly oxygenated RO_2 are fast (Berndt et al., 2018; Molteni et al., 2019). As a result, a relatively high dimer formation branching ratio of 50% was used for different RO_2 (e.g., $^{CI}RO_2$, $^{OH}RO_2$, $^{NO3}RO_2$) in the model, except for the reaction of $^{NO3}RO_2 + {}^{NO3}RO_2$, for which ROOR' dimer formation was not considered, given the extremely low signals of $CHON_2$ dimers observed in the synergistic oxidation regime (see Section 3.1). With these default kinetic parameters, the RO_2 bimolecular lifetimes were predicted to be 10.9 – 25.9 s in the O_3-only regime and 8.4 – 11.8 s in the $O_3 + NO_3$ regime in the HOM formation experiments. Considering that the RO_2 cross-reaction kinetics remain highly uncertain, sensitivity analyses were performed to evaluate their influences on the results in this study (see Section 3.2). Previous studies indicated that the primary $^{NO3}RO_2$ radicals arising from α-pinene are prone to lose the nitrate group and form pinonaldehyde with high volatility (Kurtén et al., 2017; Fry et al., 2014). Therefore, we did not

consider the autoxidation of primary $^{NO3}RO_2$ in the model. Considering the presence of NO_2 in the experiments, the reactions of $RO_2 + NO_2 \leftrightharpoons ROONO_2$ were also included in the model (Zang et al., 2023).

3. Results and Discussion

3.1 Molecular distribution of RO_2 and HOMs in the synergistic oxidation regime

The abundance of gas-phase RO_2 species and HOMs in different oxidation regimes is shown in Figure 1a. The species signals are normalized by the total reacted α-pinene in each regime. Compared to the O_3-only regime, the normalized signals of total RO_2 and HOMs decrease by 63 – 68% in the synergistic $O_3 + NO_3$ regime. Although NO_3 oxidation accounts for a considerable fraction of reacted α-pinene in the synergetic oxidation regime, the signal contributions of HOM-ONs are not significant. This might be due to the low sensitivity of nitrate-CIMS to the ONs formed involving NO_3 oxidation (Section 2.1). Although there remain considerable uncertainties in instrument sensitivities to different compounds, sensitivity analyses suggest that varying the CIMS sensitivities to RO_2 and HOMs by a factor of 10 would not significantly influence their relative distribution across different oxidation regimes (see Section S1 for details).

Note that the initial concentrations of α-pinene and O_3 in the two oxidation regimes were the same. In addition, model simulations show that in the synergistic $O_3 + NO_3$ regime, over 97% of OH radicals react with α-pinene and the depletion of OH by NO_2 is minor (0.2 – 1.3%). Also, NO_3 radicals almost entirely (over 98.5%) react with α-pinene and their reaction with RO_2 has negligible influence on the fate of RO_2 (Figure S2). Meanwhile, the depletion of acyl RO_2 by NO_2 only leads to a small reduction (4 – 5% and 7 – 12%, respectively) in total $C_xH_yO_z$-HOM monomers and dimers in the synergistic regime compared to the O_3-only regime. As a result, the strong reduction in HOM formation due to the presence of NO_3 oxidation is likely mainly due to (i) the fast competitive consumption of α-pinene by NO_3 radicals, which leads to a reduction in the reacted α-pinene by O_3 ($\Delta[\alpha\text{-pinene}]_{O3}$, Figure S3) and thereby $C_xH_yO_z$-HOM signals, and (ii) the cross reactions of $^{CI}RO_2$ or $^{OH}RO_2$ with $^{NO3}RO_2$, which suppress the autoxidation and self/cross reactions of $^{CI}RO_2$ and $^{OH}RO_2$ to form $C_xH_yO_z$-HOMs.

To quantify the contribution of cross reactions of $^{NO3}RO_2$ with $^{CI}RO_2$/$^{OH}RO_2$ to the suppressed

formation of $C_xH_yO_z$-HOMs in the synergistic oxidation regime, $C_xH_yO_z$-HOM signals shown in Figure 1a are first normalized to $\Delta[\alpha\text{-pinene}]_{O3}$ in each oxidation regime and then compared between different oxidation regimes (see Figure 1b). Notably, after excluding the influence of reduced $\Delta[\alpha\text{-pinene}]_{O3}$, the $C_xH_yO_z$-HOM signals still drop by 32 – 33% in the $O_3 + NO_3$ regime compared to those in the O_3-only regime, indicating a significant contribution of the coupled reactions between $^{NO3}RO_2$ and $^{Cl}RO_2$ or $^{OH}RO_2$ to suppressed $C_xH_yO_z$-HOM formation.

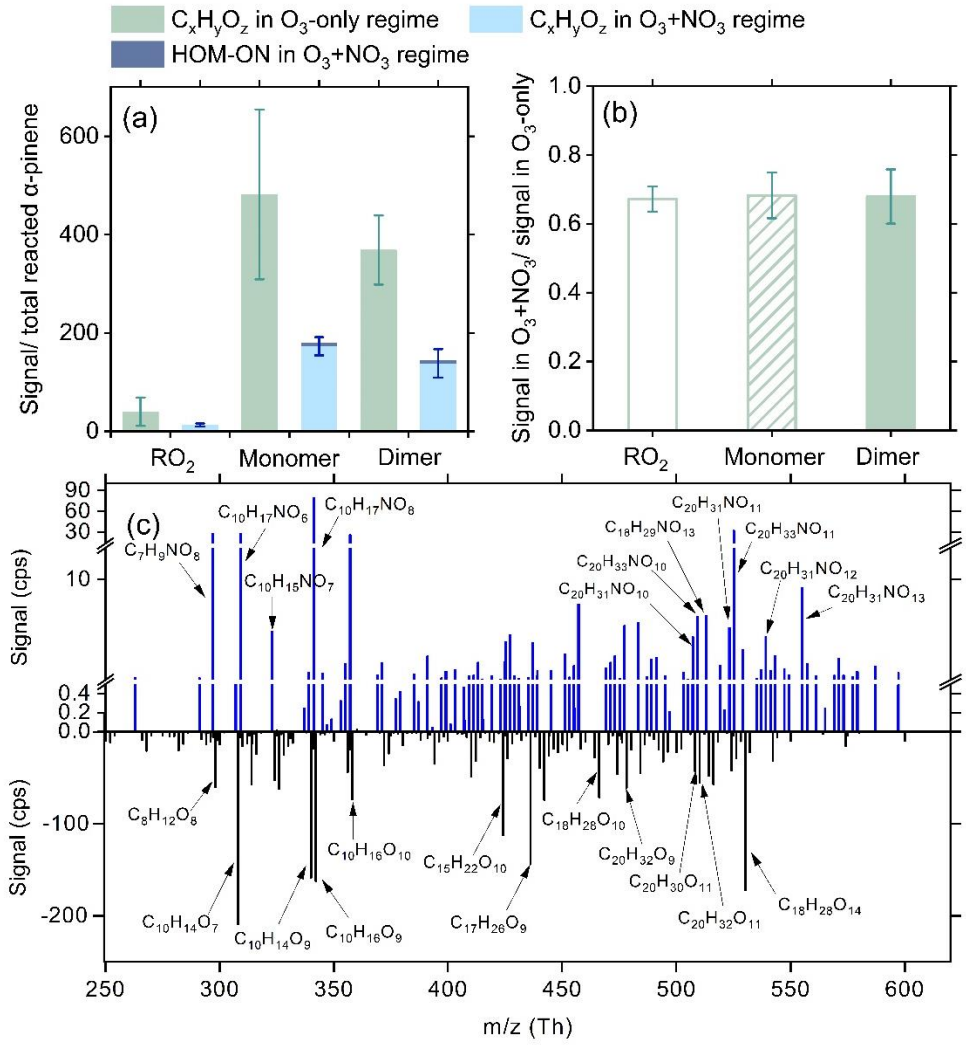

Figure 1 Distributions of RO_2 and HOMs in the O_3-only and $O_3 + NO_3$ regimes. (a) Signals of total RO_2, as well as HOM monomers and dimers normalized by the total reacted α-pinene in each oxidation regime (Exps 1-5, 7-11). (b) Relative changes in the normalized signals of $C_xH_yO_z$-HOMs in the $O_3 + NO_3$ regime versus the O_3-only regime. Ion signals are normalized to $\Delta[\alpha\text{-pinene}]_{O3}$ in each oxidation regime to highlight the suppression effect of the synergistic chemistry between $^{NO3}RO_2$ and $^{Cl}RO_2$ or $^{OH}RO_2$ on $C_xH_yO_z$-HOM formation. (c) Difference mass spectrum between the two oxidation regimes. The positive and negative peaks indicate the species with enhanced and decreased formation in the $O_3 + NO_3$ regime compared to the O_3-only regime, respectively.

Figure 1c shows a difference mass spectrum highlighting the changes in species distribution between the two oxidation regimes. Almost all $C_xH_yO_z$-HOM species decrease significantly in the O_3 + NO_3 regime compared to the O_3-only regime. Besides, a large set of HOM-ON species are formed, despite their relatively low signals. It should be noted that no obvious signals of highly oxygenated $^{NO3}RO_2$ ($C_{10}H_{16}NO_x$, $x \geq 6$) were observed by nitrate-CIMS in the O_3 + NO_3 oxidation system. One possible reason is that nitrate-CIMS exhibits relatively low sensitivity to the ONs. Secondly, the instrument's mass resolution is not high enough to differentiate the mass closure between some of $^{NO3}RO_2$ and $C_xH_yO_z$-HOMs with strong peaks (Table S2), limiting the detection of $^{NO3}RO_2$ species. Furthermore, previous studies revealed that the primary $^{NO3}RO_2$ radicals (i.e., $C_{10}H_{16}NO_5$-RO_2) in the α-pinene + NO_3 system mainly react to form pinonaldehyde (Kurtén et al., 2017; Perraud et al., 2010). It is likely that only a very small amount of $^{NO3}RO_2$ can undergo intramolecular H-shift/O_2 addition to form highly oxygenated $^{NO3}RO_2$. It should be pointed out that although the primary $C_{10}H_{16}NO_5$-RO_2 species arising from NO_3 oxidation may not undergo fast autoxidation, they tend to efficiently terminate $^{Cl}RO_2$ and/or $^{OH}RO_2$ and suppress the formation of $C_xH_yO_z$-HOMs.

As shown in Figure 1c, although several closed-shell monomeric HOM-ONs have been observed in the synergistic oxidation regime, only a few of them exhibit relatively high signals. Among them, $C_{10}H_{17}NO_8$ may be formed by the autoxidation of $C_{10}H_{16}NO_6$-RO_2 derived from the intramolecular H-shift of primary ^{NO3}RO radicals ($C_{10}H_{16}NO_4$-RO). In addition, although CI is a soft ionization method, the fragmentation of chemically labile species still occurs during the ionization in nitrate-CIMS. It is possible that some of dimeric HOM-ONs are fragmented to $C_{10}H_{17}NO_8$ during nitrate-CIMS measurements. In a recent study by Li et al. (2024), $C_{10}H_{17}NO_8$ was also identified during the synergistic oxidation of α-pinene by O_3 and NO_3. However, the exact origin of this species remains to be clarified.

The C_{20} dimers with only one nitrogen atom are very likely to be formed from the cross reactions of $^{Cl}RO_2$ or $^{OH}RO_2$ with $^{NO3}RO_2$, which provides direct evidence for the synergistic RO_2 chemistry in the O_3 + NO_3 regime. The $CHON_2$ dimers were also observed in the O_3 + NO_3 regime, despite their much lower signals than CHON dimers, which is different from the recent studies by Bates et al. (2022) and Li et al. (2024), which found $CHON_2$ dimers account for an important fraction of the

total dimer signals in the synergistic oxidation regime. A potential explanation for this discrepancy is the difference in the instrument sensitivity in these studies (Section 2.1). In general, the nitrate-CIMS has lower sensitivities to ONs than to the $C_xH_yO_z$-HOM counterparts (Shen et al., 2022; Hyttinen et al., 2015). Bates et al. (2022) used CF_3O^- as the reagent ion of CIMS. Its sensitivity to ONs might be significantly higher than the nitrate ion. In addition, Li et al. (2024) observed a significantly lower signal contribution of $CHON_2$ dimers using CI-Orbitrap with nitrate reagent ions than with ammonium ions. Despite both using nitrate reagent ions, the nitrate CI-Orbitrap in Li et al. (2024) possibly exhibits higher sensitivities to ONs than the nitrate-CIMS in our study.

3.2 Synergistic reaction efficiencies of different RO_2 species

In the $O_3 + NO_3$ regime, synergistic reactions are likely to occur between $^{CI}RO_2$, $^{OH}RO_2$ and $^{NO3}RO_2$. Figure 2 shows the $\Delta[\alpha\text{-pinene}]_{O3}$-normalized signal ratios of specific C_{10} RO_2 as well as their related $C_xH_yO_z$-HOM monomers and dimers in the synergistic $O_3 + NO_3$ regime vs. the O_3-only regime. It should be noted that the second-generation oxidation processes are strongly inhibited by the excess of α-pinene in this study, thus the predominant type of RO_2 observed here is primary RO_2. Model simulations show that the H-abstraction of α-pinene by OH radicals contributes less than 2% to the formation of $C_{10}H_{15}O_x$-RO_2 and related HOMs under different experimental conditions (Figure S5). Therefore, $C_{10}H_{15}O_x$-RO_2 observed in this study are primarily $^{CI}RO_2$. Notably, the $^{CI}RO_2$ ($C_{10}H_{15}O_x$) and related $C_{10}H_{14}O_x$-HOMs decrease by ~20 – 80% in the $O_3 + NO_3$ regime (Figures 2 a, b), while the decreasing extent of $^{OH}RO_2$ ($C_{10}H_{17}O_x$) and related $C_{10}H_{18}O_x$-HOMs are significantly smaller (0 – 30%). In particular, some of the most oxygenated $C_{10}H_{17}O_x$-RO_2 and $C_{10}H_{18}O_x$-HOMs ($x \geq 9$) even increase unexpectedly in the synergistic oxidation regime. For the $C_{10}H_{16}O_x$-HOMs that can be derived from the self/cross reactions of both $^{CI}RO_2$ and $^{OH}RO_2$, their reductions are at a medium level. Because of the very small contribution of acyl RO_2 to the total C_{10} RO_2 (0.4%) (Zang et al., 2023), their consumption by NO_2 leads to less than 2% reduction in the C_{10} $^{CI}RO_2$ signals. Therefore, the more significant decrease in signals of $^{CI}RO_2$ and related HOMs as compared to the OH-derived ones in the synergistic $O_3 + NO_3$ regime is primarily due to the more efficient cross reactions of $^{NO3}RO_2$ with $^{CI}RO_2$ than with $^{OH}RO_2$. Because a large amount of $^{CI}RO_2$ is terminated by $^{NO3}RO_2$, fewer $^{CI}RO_2$ are available to terminate $^{OH}RO_2$. As a result, more $^{OH}RO_2$ can undergo autoxidation to form highly oxygenated $C_{10}H_{17}O_x$-RO_2 and $C_{10}H_{18}O_x$-HOMs ($x \geq 9$),

leading to an increase in signals of these species. Consistently, the signals of C_{20} HOM dimers decrease by ~20 – 40% in the O_3 + NO_3 regime compared to that in O_3-only regime, and the signal reduction of dimers ($C_{20}H_{30}O_x$) formed by $^{Cl}RO_2$ is slightly larger than that of the dimers ($C_{20}H_{34}O_x$) arising from $^{OH}RO_2$ (Figure 2c). Note that the highly oxygenated $C_{20}H_{34}O_x$ dimers (x ≥ 13) that can be formed from self/cross reactions of $C_{10}H_{17}O_x$-RO_2 (x ≥ 9) are not observed in this study, likely due to their low abundance and the limitation of instrument sensitivity.

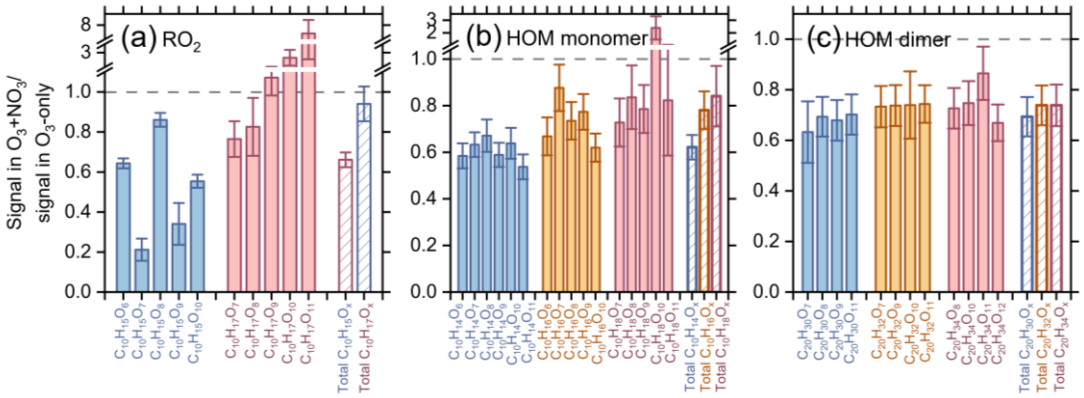

Figure 2. Normalized signal ratios of (a) specific and total $C_{10}H_{15,17}O_x$-RO_2 radicals, as well as their related (b) C_{10} HOM monomers and (c) C_{20} HOM dimers in the O_3 + NO_3 regime vs. the O_3-only regime (Exps 1-5, 7-11). Ion signals observed in each oxidation regime are normalized to $\Delta[\alpha\text{-pinene}]_{O3}$.

The above results are somewhat different from the most recent study by Li et al. (2024), which found that the measured $C_{10}H_{15}O_x$-RO_2 increased slightly with NO_3 radicals while $C_{10}H_{17}O_{5,7}$-RO_2 from OH chemistry decreased by a factor of 9. Li et al. (2024) indicated that additional $C_{10}H_{15}O_x$ could be produced from the H-abstraction pathway of NO_3 oxidation of α-pinene. However, in the monoterpene oxidation system, the rate constant for H-abstraction by NO_3 radicals is $(4 – 10) \times 10^{-17}$ cm^3 $molecule^{-1}$ s^{-1}, which is $10^3 – 10^4$ times lower than that for the NO_3 addition channel (Martinez et al., 1998). Besides, the subsequent reactions of RO_2 species formed from H-abstraction by NO_3 radicals should be very similar to those derived from H-abstraction by OH radicals, which was found not important for $C_xH_yO_z$-HOM formation in the absence of NO (Zang et al., 2023). Therefore, the H-abstraction of α-pinene by NO_3 radicals would have negligible influence on $C_{10}H_{15}O_x$ formation. As Li et al. (2024) used a low α-pinene concentration and relatively high O_3 and NO_3 concentrations in their experiments, the secondary oxidation of aldehydes, such as the substantially formed pinonaldehyde, by NO_3 radicals might be important, which could contribute to the additional

328 formation of $C_{10}H_{15}O_x$-RO_2. However, as noted above, the second-generation oxidation processes
329 are strongly inhibited due to the excess of α-pinene in this study, therefore the formation of
330 secondary $C_{10}H_{15}O_x$-RO_2 is not important.

331 In addition, Li et al. (2024) reported that the fraction of α-pinene oxidized by OH radicals decreased
332 from 44% in the O_3 oxidation system to 6% in the O_3 + NO_3 system, mainly due to the depletion of
333 OH radicals by NO_2 and the competitive consumption of α-pinene by NO_3 radicals, which resulted
334 in a significant decrease in $C_{10}H_{17}O_{5,7}$ radicals from OH chemistry as observed in their experiments.
335 However, in the present study, because of the excess of α-pinene, over 97% of OH radicals react
336 with α-pinene and the depletion of OH by NO_2 is minor (0.2 – 1.3%) in the O_3 + NO_3 regime. The
337 reduction in the reacted α-pinene by OH radicals is less than 10% compared to the O_3-only regime.
338 As a result, a smaller decrease in $C_{10}H_{17}O_{5,7}$ radicals was observed in our study.

339 To gain quantitative constraints on the relative reaction efficiency of $^{NO3}RO_2$ + $^{CI}RO_2$ vs. $^{NO3}RO_2$ +
340 $^{OH}RO_2$ (i.e., k_{NO3+CI}/k_{NO3+OH}), the signal ratios of C_{10}-$^{CI}RO_2$ and $^{OH}RO_2$ as well as their related C_{10}
341 HOMs in the synergistic oxidation regime vs. the O_3-only regime were predicted using a kinetic
342 model (see Section 2.3) with different k_{NO3+CI}/k_{NO3+OH} ratios. Figure 3 shows a measurement-model
343 comparison of those signal ratios. When the ratio of k_{NO3+CI}/k_{NO3+OH} is smaller than or equal to 1,
344 the simulated signal ratios of many RO_2 and HOMs differ significantly from the measured ratios,
345 especially for some $C_{10}H_{17}O_x$-RO_2 and $C_{10}H_{18}O_x$-HOMs. When the ratio of k_{NO3+CI}/ k_{NO3+OH} is 10 –
346 100, there is a good measurement-model agreement for most of RO_2 and HOMs. Therefore, we
347 conclude that the cross-reaction rate constants of $^{NO3}RO_2$ + $^{CI}RO_2$ are on average 10 – 100 times
348 larger than those for $^{NO3}RO_2$ + $^{OH}RO_2$. This different RO_2 cross-reaction efficiency is the main
349 reason for the significantly larger decrease in the abundance of $^{CI}RO_2$ and related HOMs as
350 compared to the OH-derived ones (see Figure 2).

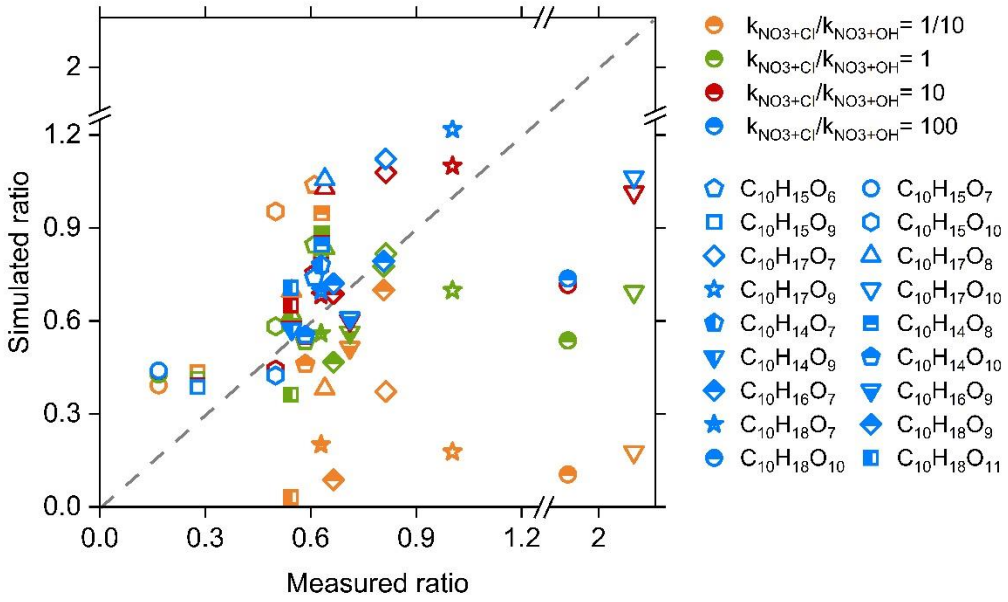

Figure 3. Measurement-model comparisons of the signal ratios of different C_{10} RO_2 and HOMs in the synergistic O_3 + NO_3 regime vs. the O_3-only regime. The cross-reaction rate constant of $^{NO3}RO_2$ + $^{Cl}RO_2$ was set to 2 × 10^{-12} cm^3 $molecule^{-1}$ s^{-1} and the rate of $^{NO3}RO_2$ + $^{OH}RO_2$ was varied from 2 × 10^{-11} cm^3 $molecule^{-1}$ s^{-1} to 2 × 10^{-14} cm^3 $molecule^{-1}$ s^{-1} in the model.

As a competitive reaction pathway, the autoxidation rates of RO_2 can affect the extent to which RO_2 cross reactions influence the RO_2 fate and HOM formation. Therefore, sensitivity analyses of the autoxidation rate of RO_2 were conducted to evaluate its influence on the changes of RO_2 and related HOM concentrations in the synergistic O_3 + NO_3 regime vs. the O_3-only regime (Figure S6). In these analyses, a k_{NO3+Cl}/k_{NO3+OH} ratio of 10 was used according to the above discussions. As the autoxidation rate of $^{OH}RO_2$ increases from 0.28 to 10 s^{-1}, corresponding to the rate range reported in previous studies (Berndt et al., 2016; Zhao et al., 2018; Xu et al., 2019), the simulated reduction of highly oxygenated $^{OH}RO_2$ and related $C_{10}H_{18}O_x$-HOMs in the synergistic O_3 + NO_3 regime exhibits a slight decrease (< 10%) but still agrees reasonably well with the measured value (Figures S6 a-d). Considering that the autoxidation rates of $^{Cl}RO_2$ used in the model approach their upper limits reported in the literature, i.e., ~1 s^{-1} for the butyl ring-opened $C_{10}H_{15}O_4$-RO_2 (Iyer et al., 2021) and relatively smaller rates for ring-retained $C_{10}H_{15}O_4$-RO_2 (0.02 – 0.29 s^{-1}, see Scheme S1) (Zhao et al., 2021), we also lowered the autoxidation rate constants of $^{Cl}RO_2$ by a factor of 10 to see its influence on RO_2 and HOM distribution in the O_3 + NO_3 regime. The simulated reduction of $^{Cl}RO_2$ and $C_{10}H_{14}O_x$-HOMs in this case decreases by 7 – 16% (Figures S6 e-h), while that of $C_{10}H_{16}O_x$-HOMs increases by up to 31% (Figures S6 i, j). However, the simulated results are still close to the

measured values. These sensitivity analyses suggest that the uncertainty in the autoxidation rates of $^{OH}RO_2$ and $^{Cl}RO_2$ could slightly affect the simulated distribution of RO_2 and HOMs across different oxidation regimes but not significantly change the k_{NO3+Cl}/k_{NO3+OH} ratio obtained in this study. Further sensitivity analyses on the rate constant and dimer formation branching ratio of RO_2 cross reactions indicate that the uncertainties in these reaction kinetics do not alter the conclusion regarding the k_{NO3+Cl}/k_{NO3+OH} ratio either (see details in Sections S2 and S3).

Cyclohexane was added in some experiments as an OH scavenger to elucidate the role of $^{OH}RO_2$ chemistry in HOM formation in the O_3 + NO_3 regime. In the presence of cyclohexane, most of $^{OH}RO_2$ ($C_{10}H_{17}O_x$) and related HOM monomers ($C_{10}H_{18}O_x$) and dimers ($C_{20}H_{32}O_x$ and $C_{20}H_{34}O_x$) decrease by more than 70% (Figure 4), while $^{Cl}RO_2$ ($C_{10}H_{15}O_x$) and related HOM monomers ($C_{10}H_{14}O_x$) only decrease slightly. Accordingly, the reduction in $C_{20}H_{32}O_x$ and $C_{20}H_{34}O_x$ dimers is significantly larger than that of $C_{20}H_{30}O_x$. These results are in a good agreement with previous measurements (Zhao et al., 2018; Zang et al., 2023). The $C_{10}H_{16}O_x$ species, which can arise from both $^{Cl}RO_2$ and $^{OH}RO_2$, exhibit a medium reduction (Figure 4b). It is interesting to note that with the addition of cyclohexane, there is a significant increase in $C_{20}H_{31}NO_x$, which are formed from the cross reactions of $^{Cl}RO_2$ with $^{NO3}RO_2$. Such an enhanced production of $C_{20}H_{31}NO_x$ as compared to the slightly deceased formation of $C_{20}H_{30}O_x$ indicates that the $^{Cl}RO_2$ + $^{NO3}RO_2$ reactions are competitive compared to the $^{Cl}RO_2$ + $^{Cl}RO_2$ and $^{Cl}RO_2$ + $^{OH}RO_2$ reactions. As a result, when the $^{OH}RO_2$ are depleted, the $^{Cl}RO_2$ that are supposed to react with $^{OH}RO_2$, efficiently react with $^{NO3}RO_2$ to form $C_{20}H_{31}NO_x$, leading to the increase in $C_{20}H_{31}NO_x$ signals. Consistent with the experimental measurements, the model simulations show that the concentrations of $C_{20}H_{31}NO_x$ in the O_3 + NO_3 regime increase with the addition of cyclohexane as an OH scavenger (Figure S9). However, the simulated enhancement is slightly lower than the measurements, which might be due to the uncertainties in the RO_2 cross-reaction kinetics in the model.

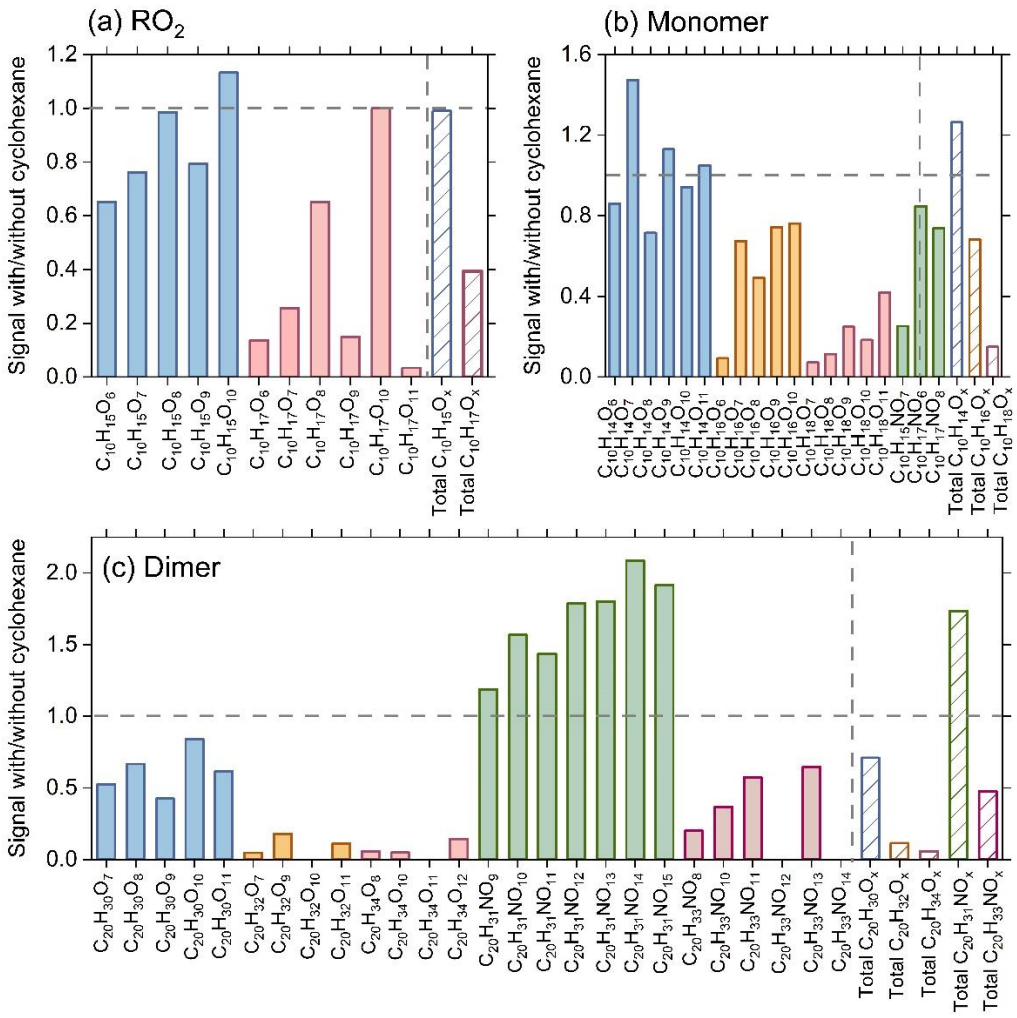

Figure 4. Relative changes in signals of (a) C_{10} RO_2, (b) C_{10} HOMs, and (c) C_{20} dimers due to the addition of 100 ppm cyclohexane as an OH scavenger derived in the synergistic O_3 + NO_3 regime (Exps 6 and 12).

3.3 Influence of synergistic oxidation on low-volatility organics and particle formation

Compared to the O_3-only regime, there are a remarkable reduction in $C_xH_yO_z$-HOMs and a strong formation of HOM-ONs due to the efficient cross reactions between $^{NO3}RO_2$ and $^{Cl}RO_2$ in the synergistic oxidation regime. This significant change in HOM composition and abundance would alter the volatility distribution of HOMs and influence the formation of particles. The volatilities of HOMs formed in the two oxidation regimes are estimated using a modified composition-activity method (see Section 2.2) and shown in Figure 5. The abundance of $C_xH_yO_z$-HOMs characterized as ULVOCs and ELVOCs decreases considerably in the synergistic O_3 + NO_3 regime compared to the O_3-only regime (Figure 5), in agreement with the very recent observations by Li et al. (2024) who found that the presence of NO_3 radicals during α-pinene ozonolysis significantly reduced the

abundance of ULVOCs. Although substantial amounts of HOM-ONs are formed in the O_3 + NO_3 regime, they generally have higher volatilities (i.e., characterized as ELVOCs to IVOCs) (Figure 5). Therefore, the synergistic O_3 + NO_3 oxidation of α-pinene significantly reduces the formation of ULVOCs and increases the overall volatility of total HOMs.

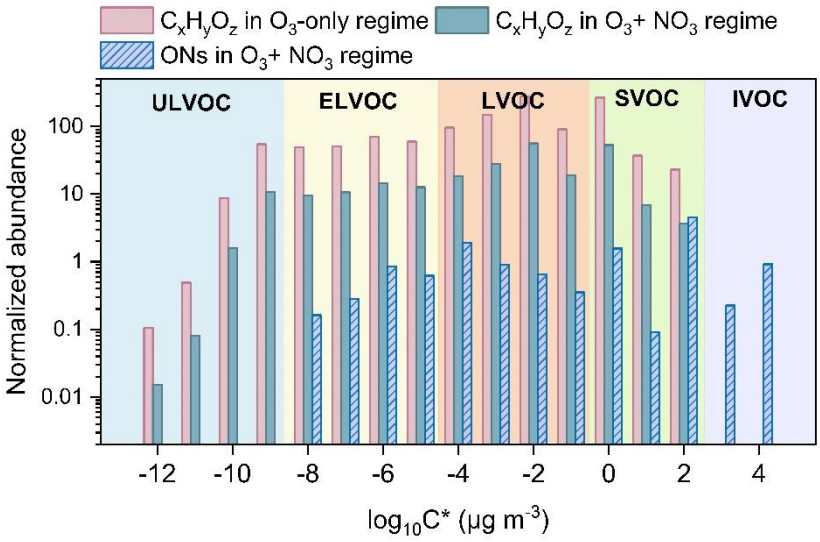

Figure 5. Volatility distribution of $C_xH_yO_z$-HOMs and HOM-ONs formed in the O_3 + NO_3 regime and O_3-only regime (Exps 1, 7). Ion signals in each oxidation regime are normalized to the corresponding total reacted α-pinene.

Figure 6a shows the particle number and mass concentrations formed in the two oxidation regimes in SOA formation experiments (Exps 13, 14). The particle number concentration decreases by ~50% whereas the particle mass concentration increases by a factor of 2 in the synergistic O_3 + NO_3 regime, compared to that in the O_3-only regime. The presence of NO_3 radicals during α-pinene ozonolysis reduces the abundance of ULVOCs, which are the key species driving particle nucleation, thereby leading to a reduction in the particle number concentration in the O_3 + NO_3 regime. On the other hand, substantial formation of HOM-ONs is expected from the cross reactions of $^{NO3}RO_2$ with $^{CI}RO_2$ and $^{OH}RO_2$ in the synergistic oxidation regime (Li et al., 2024; Bates et al., 2022), although their signals are relatively low due to the low sensitivity of nitrate-CIMS to ONs in this study. The newly formed HOM-ONs have relatively higher volatilities and are inefficient in initiating particle nucleation, but they are able to partition into the formed particles and contribute to the particle mass growth. Meanwhile, as the particle number concentration decreases drastically in the synergistic oxidation regime, more condensable vapors are available for each particle to grow to larger sizes (Figure 6b), which would in turn favor the condensation of more volatile organic species including

ONs due to the reduced curvature effect of the larger particles, ultimately resulting in an increase in SOA mass concentrations.

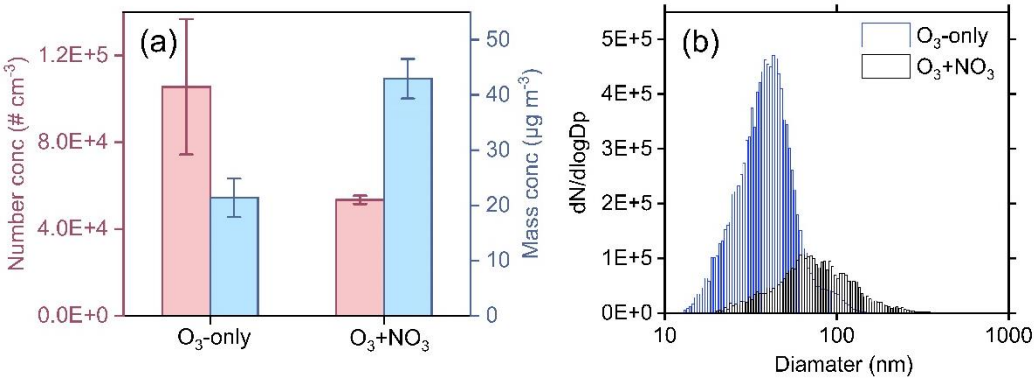

Figure 6. Number and mass concentrations (a), as well as the size distribution (b) of particles formed from the ozonolysis and synergistic O_3 + NO_3 oxidation of α-pinene (Exps 13-14).

Recently, Bates et al. (2022) also found that in chamber experiments with seed particles, the SOA mass yields were significantly higher during α-pinene oxidation by O_3 + NO_3 than during ozonolysis, mainly due to the substantial formation and condensation of dimeric ONs. However, in the absence of seed particles, synergistic O_3 + NO_3 oxidation of α-pinene does not nucleate in their study. This phenomenon might be due to the high concentrations of NO_2 (72 ppb) and O_3 (102 ppb) as well as the relatively low concentration of α-pinene (27 ppb) in their experiments. As indicated by Bates et al. (2022), under this conditions NO_3 radicals were substantially formed and contributed to a dominant fraction (75%) of α-pinene oxidation, which strongly inhibited the production of low-volatility species and particle nucleation.

3.4 Atmospheric relevance of experimental results

In the present study, the flow tube experiments were conducted under dry conditions. Although water vapor may affect the fate of Criegee intermediates and RO_2 radicals and thereby HOM formation during the oxidation of organics under humid conditions, there is growing evidence that such effects in the α-pinene oxidation system are small. Kinetics studies have found that the stabilized Criegee intermediates (SCIs) arising from α-pinene ozonolysis can undergo fast unimolecular decay at a rate constant of 60 – 250 s^{-1} (Vereecken et al., 2017; Newland et al., 2018), which is rapid compared to their reaction with water vapor, in particular for syn-SCIs, under atmospheric conditions (Vereecken et al., 2017; Newland et al., 2018). In addition, the yield of OH

radicals from Criegee decomposition is independent of RH (Atkinson et al., 1992; Aschmann et al., 2002). Consistent with the fast unimolecular reaction kinetics revealed by these studies, recent laboratory measurements have shown that the contribution of SCIs to the formation of gas-phase and particle-phase dimers are small (<20%) during α-pinene ozonolysis (Zhao et al., 2018; Zhao et al., 2022). Furthermore, the molecular composition and abundance of HOM monomers and dimers (Li et al., 2019) and the formation of particle-phase dimers (Zhang et al., 2015; Kenseth et al., 2018) do not change significantly with RH ranging from 3% to 92%. These studies suggest that the humidity condition does not strongly affect the HOM formation chemistry in the α-pinene ozonolysis system.

To evaluate the relevance of our experimental findings to the real atmosphere, we performed chemical model simulations of HOM formation from nocturnal synergistic O_3 + NO_3 oxidation of α-pinene under typical atmospheric conditions. In these simulations, constant concentrations of α-pinene (1 ppb), O_3 (30 ppb), NO (5 ppt), NO_2 (1.8 ppb), NO_3 radicals (0.2 or 1 ppt), OH radicals (5 – 50 $\times 10^4$ molecules cm^{-3}), HO_2 radicals (4 ppt), as well as a constant RH of 50% and temperature of 298 K were used as typical nocturnal conditions in the boreal forest according to the field studies (Stone et al., 2012; Lee et al., 2016a; Brown and Stutz, 2012; Geyer et al., 2003b; Kristensen et al., 2016; Hakola et al., 2012; Liebmann et al., 2018). Considering the rapid deposition of oxidized biogenic compounds (Nguyen et al., 2015), a typical dilution lifetime of 5 h (i.e., k_{dil} = 1/5 h^{-1}) was assumed in the model. According to the above analysis, the cross-reaction rate constants for $^{NO3}RO_2$ + $^{Cl}RO_2$ and $^{NO3}RO_2$ + $^{OH}RO_2$ were set to 2 $\times 10^{-12}$ cm^3 $molecule^{-1}$ s^{-1} and 2 $\times 10^{-13}$ cm^3 $molecule^{-1}$ s^{-1} in the model, respectively. The formation of RO_2 with oxygen numbers higher than 11 was not considered in the model, due to the large uncertainty in the autoxidation rate constants of the highly oxygenated RO_2. In fact, the autoxidation rate of the highly oxygenated RO_2 is expected to be small given the significant decrease in the number of active sites for intramolecular H-abstraction in the molecule. As a result, the contribution of the most oxygenated HOMs to the total HOM monomers could be relatively small (Zhao et al., 2018; Claflin et al., 2018).

In the absence of NO_3 radicals (with NO_3 concentrations and formation rates set to zero), the amount of α-pinene consumed during 4 hours of simulation is 1.04 ppb. When a relatively low NO_3 concentration (0.2 ppt) is considered (Figure 7a), the amount of α-pinene consumed is 1.48 ppb, and

485 the ozonolysis is the primary loss pathway of α-pinene (68%), followed by NO_3 (30%) and OH
486 oxidation (2%). The reactions of RO_2 + HO_2, RO_2 + NO, and RO_2 + RO_2 account for ~49%, ~27%,
487 and ~24% of the total RO_2 fate, respectively (Figure S10a). Compared to the ozonolysis of α-pinene,
488 the synergistic O_3 + NO_3 oxidation leads to a reduction of 3% and 13% in the formation of $C_xH_yO_z$-
489 HOM monomers and dimers, respectively (Figure 7b). Given that the concentrations of α-pinene
490 and oxidants were held constant during the simulation, the consumptions of α-pinene by O_3 and OH
491 radicals are the same across different oxidation regimes. Therefore, the decreases in the
492 concentrations of $C_xH_yO_z$-HOM monomers and dimers in the presence of NO_3 oxidation are mainly
493 due to the cross reactions of $^{NO3}RO_2$ with other RO_2. When the NO_3 concentration is as high as 1
494 ppt as reported in field studies (Liebmann et al., 2018), the consumption of α-pinene reaches 3.24
495 ppb, of which 68% is contributed by NO_3 oxidation (Figure 7c). Under this condition, the RO_2 +
496 RO_2 reactions account for ~34% of the total RO_2 fate (Figure S10b). As a result, the cross reactions
497 of $^{NO3}RO_2$ with other RO_2 play a more important role in the HOM formation. The production of
498 $C_xH_yO_z$-HOM monomers and dimers decreases by 12% and 43%, respectively, due to the presence
499 of NO_3 oxidation (Figure 7d). We note that the variation in RH from 0 – 90% in the model has
500 negligible influence on the relative changes in $C_xH_yO_z$-HOMs under these nocturnal atmospheric
501 conditions (Figure S11). Considering that there are uncertainties in the dilution rate constant, a
502 sensitivity analysis was performed by varying the k_{dil} in the range of 0.04 – 0.2 h^{-1}. It is found that
503 the variation within these rate values does not significantly influence the response of $C_xH_yO_z$-HOM
504 dimer formation to concurrent NO_3 oxidation (Figure S12).

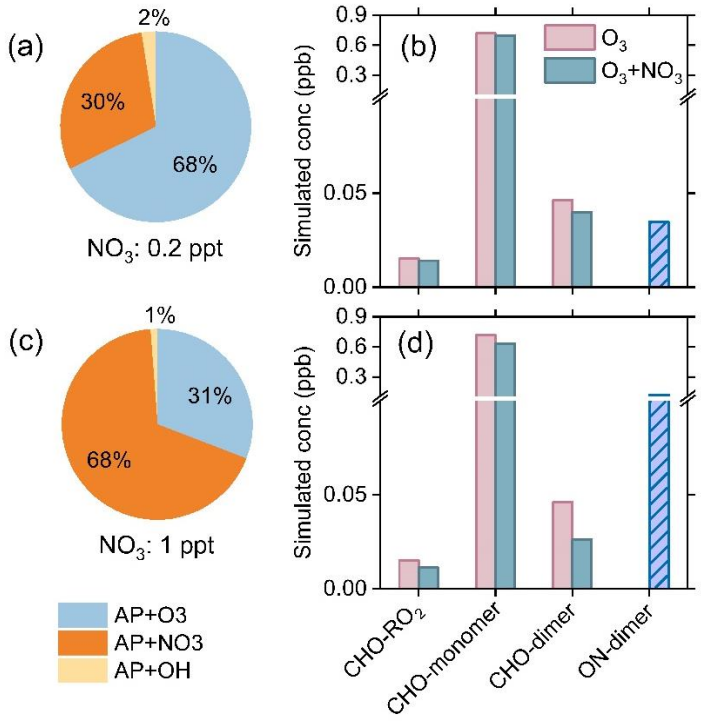

Figure 7. Model simulations of α-pinene oxidation and HOM formation under typical nighttime conditions in the boreal forest. (a, c) Contributions of different loss pathways of α-pinene by different oxidants at NO_3 concentrations of 0.2 and 1 ppt, respectively; (b, d) Concentrations of $C_xH_yO_z$-HOMs and HOM-ONs formed by synergistic O_3 + NO_3 oxidation and ozonolysis of α-pinene under conditions corresponding to (a) and (c). The simulations were run for 4 h after an 8-h spin-up for intermediates and secondary species.

Field observations have shown that NO_3 radicals, O_3, and OH radicals all had important contributions to monoterpene oxidation during the early morning after sunrise and late afternoon before sunset in the southeastern United States (Zhang et al., 2018). In addition, relatively high nighttime OH concentrations of (2 – 10) × 10^5 molecules cm^{-3} were measured in some areas such as Germany and New York City (Faloona et al., 2001; Geyer et al., 2003a). As a result, a model simulation was conducted using a 10 times higher OH concentration (5 × 10^5 molecules cm^{-3}). The concentration of NO_3 radicals is 1 ppt and the concentrations of other species are the same as the values mentioned above. With a higher OH concentration, O_3, NO_3, and OH radicals account for 28%, 61%, and 11% to the total α-pinene consumption, respectively (Figure S13 a). Compared to the results under low OH concentration, the formation of $C_xH_yO_z$-HOM monomers and dimers are all enhanced under high OH concentration (Figure S13 b). This is mainly due to the promoted self/cross reactions of $^{OH}RO_2$, as well as the promoted formation of $C_{10}H_{15}O_x$-RO_2 derived from H-abstraction pathway by OH radicals. Nevertheless, the presence of NO_3 oxidation still reduces the

formation of $C_xH_yO_z$-HOM dimers by 26% (Figure S13 b).

Furthermore, model simulations under typical conditions in the southeastern United States (see details in Section S4) suggest that the coexistence of isoprene appears to exacerbate the suppression effect of synergistic oxidation on HOM formation from monoterpenes. As shown in Figure S14, in the absence of isoprene, the synergistic O_3 + NO_3 oxidation of α-pinene leads to a reduction of 13% and 24% in the formation of $C_xH_yO_z$-HOM monomers and dimers, respectively. When isoprene is present, as the isoprene + NO_3 oxidation produces a significant amount of nitrooxy RO_2 that can also scavenge α-pinene-derived $^{CI}RO_2$ and $^{OH}RO_2$ via cross reactions, the synergistic oxidation leads to a slightly larger reduction in $C_xH_yO_z$-HOM monomers and dimers (15% and 31%, respectively).

The above model simulations suggest that under nocturnal atmospheric conditions with a very low NO_3 concentration, the RO_2 radical pool is dominated by $^{CI}RO_2$ and their self/cross reactions are a major contributor to ULVOCs such as the highly oxygenated C_{20} dimers as observed in boreal forest (Bianchi et al., 2017). When the NO_3 concentration is high, the production of $^{NO3}RO_2$ becomes significant and their cross reactions with $^{CI}RO_2$ would suppress the formation of ULVOCs. Although HOM-ON dimers are readily produced by cross reactions between $^{NO3}RO_2$ and $^{CI}RO_2$, they generally have higher volatilities than $C_xH_yO_z$-HOM dimers and therefore are less efficient in initiating particle formation. However, these HOM-ONs can be an important contributor to the particle mass growth. As suggested by the model simulations in Bates et al. (2022), the NO_3 oxidation of α-pinene led to a particulate nitrate yield of 7% under nocturnal atmospheric conditions in rural Alabama during the SOAS campaign. Our results offer mechanistic and quantitative insights on how the synergistic oxidation of α-pinene by O_3 and NO_3 radicals can influence the formation of low-volatility organic compounds and hence particle formation and growth. They also provide a potential explanation for field observations that NPF events frequently occur in monoterpene-rich regions during daytime but not at nighttime (Mohr et al., 2017; Kulmala et al., 2001; Junninen et al., 2017).

4. Conclusions

This study provides a comprehensive characterization of the nocturnal synergistic oxidation of α-pinene by O_3 and NO_3 radicals and its influence on the formation of HOMs and low-volatility organic compounds using a combination of flow reactor experiments and detailed kinetic model simulations. It is found that the formation of $C_xH_yO_z$-HOMs in the O_3 + NO_3 regime is significantly

suppressed compared to that in the O_3-only regime, mainly due to the depletion of ozonolysis-derived RO_2 (i.e., $^{CI}RO_2$ and $^{OH}RO_2$) by $^{NO3}RO_2$ via cross reactions. In addition, the decreases in the abundance of $^{CI}RO_2$ and related HOMs are significantly larger than those of OH-derived ones, indicating that the $^{NO3}RO_2$ species react more efficiently with $^{CI}RO_2$ than with $^{OH}RO_2$. Detailed measurement-model comparisons for the distribution of a suite of $^{CI}RO_2$, $^{OH}RO_2$, and associated HOMs across different oxidation regimes further reveal that the cross reactions between $^{CI}RO_2$ and $^{NO3}RO_2$ are averagely 10 – 100 times more efficient than those of $^{OH}RO_2$ and $^{NO3}RO_2$.

The suppressed formation of $C_xH_yO_z$-HOMs in the synergistic O_3 + NO_3 regime results in a significant reduction in ULVOCs. Although substantial amounts of HOM-ONs are formed from the cross reactions between $^{NO3}RO_2$ and $^{CI}RO_2$ or $^{OH}RO_2$ in the synergistic oxidation regime, they have higher volatilities and are less likely to participate in the formation and initial growth of new particles. As a result, in our experiment the formation of new particles in the synergistic oxidation regime is substantially inhibited compared to the O_3-only regime. Chemical model simulations further confirm that the synergistic oxidation of α-pinene by O_3 and NO_3 radicals can significantly inhibit the formation of $C_xH_yO_z$-HOMs, especially the ultra-low volatility $C_xH_yO_z$-HOM dimers under typical nighttime atmospheric conditions. Our study sheds lights on the synergistic oxidation mechanism of biogenic emissions and underscores the importance of considering this chemistry for a better depiction of the formation of low-volatility organics and particles in the atmosphere.

Data availability. The data presented in this work are available upon request from the corresponding author.

Author contributions. YZ and HZ designed the study, HZ and DH performed the experiments. YZ and HZ analyzed the data, conducted model simulations, and wrote the paper. All other authors contributed to discussion and writing.

Competing interests. The authors declare no conflict of interest.

Acknowledgments. This work was supported by the National Natural Science Foundation of China (grants 22376137 and 22022607). Dan Dan Huang acknowledges the financial support from the Science and Technology Commission of Shanghai Municipality (grant 21230711000).

References

Aschmann, S. M., Arey, J., and Atkinson, R.: OH radical formation from the gas-phase reactions of O_3 with a series of terpenes, Atmos. Environ., 36, 4347-4355, https://doi.org/10.1016/S1352-2310(02)00355-2, 2002.

Atkinson, R., Aschmann, S. M., Arey, J., and Shorees, B.: Formation of OH radicals in the gas-phase reactions of O_3 with a series of terpenes, J. Geophys. Res.-Atmos., 97, 6065-6073, https://doi.org/10.1029/92JD00062, 1992.

Ayres, B. R., Allen, H. M., Draper, D. C., Brown, S. S., Wild, R. J., Jimenez, J. L., Day, D. A., Campuzano-Jost, P., Hu, W., de Gouw, J., Koss, A., Cohen, R. C., Duffey, K. C., Romer, P., Baumann, K., Edgerton, E., Takahama, S., Thornton, J. A., Lee, B. H., Lopez-Hilfiker, F. D., Mohr, C., Wennberg, P. O., Nguyen, T. B., Teng, A., Goldstein, A. H., Olson, K., and Fry, J. L.: Organic nitrate aerosol formation via NO_3 + biogenic volatile organic compounds in the southeastern United States, Atmos. Chem. Phys., 15, 13377-13392, https://doi.org/10.5194/acp-15-13377-2015, 2015.

Bates, K. H., Burke, G. J. P., Cope, J. D., and Nguyen, T. B.: Secondary organic aerosol and organic nitrogen yields from the nitrate radical (NO_3) oxidation of alpha-pinene from various RO_2 fates, Atmos. Chem. Phys., 22, 1467-1482, https://doi.org/10.5194/acp-22-1467-2022, 2022.

Berndt, T.: Peroxy radical processes and product formation in the OH radical-initiated oxidation of alpha-pinene for near-atmospheric conditions, J. Phys. Chem. A, 125, 9151-9160, https://doi.org/10.1021/acs.jpca.1c05576, 2021.

Berndt, T., Mentler, B., Scholz, W., Fischer, L., Herrmann, H., Kulmala, M., and Hansel, A.: Accretion product formation from ozonolysis and OH radical reaction of alpha-pinene: mechanistic insight and the influence of isoprene and ethylene, Environ. Sci. Technol., 52, 11069-11077, https://doi.org/10.1021/acs.est.8b02210, 2018.

Berndt, T., Richters, S., Jokinen, T., Hyttinen, N., Kurtén, T., Otkjær, R. V., Kjaergaard, H. G., Stratmann, F., Herrmann, H., Sipilä, M., Kulmala, M., and Ehn, M.: Hydroxyl radical-induced formation of highly oxidized organic compounds, Nat. Commun., 7, https://doi.org/10.1038/ncomms13677, 2016.

Bianchi, F., Garmash, O., He, X. C., Yan, C., Iyer, S., Rosendahl, I., Xu, Z. N., Rissanen, M. P., Riva, M., Taipale, R., Sarnela, N., Petäjä, T., Worsnop, D. R., Kulmala, M., Ehn, M., and Junninen, H.: The role of highly oxygenated molecules (HOMs) in determining the composition of ambient ions in the boreal forest, Atmos. Chem. Phys., 17, 13819-13831, https://doi.org/10.5194/acp-17-13819-2017, 2017.

Bianchi, F., Kurtén, T., Riva, M., Mohr, C., Rissanen, M. P., Roldin, P., Berndt, T., Crounse, J. D., Wennberg, P. O., Mentel, T. F., Wildt, J., Junninen, H., Jokinen, T., Kulmala, M., Worsnop, D. R., Thornton, J. A., Donahue, N., Kjaergaard, H. G., and Ehn, M.: Highly oxygenated organic molecules (HOM) from gas-phase autoxidation involving peroxy radicals: a key contributor to atmospheric aerosol, Chem. Rev., 119, 3472-3509, https://doi.org/10.1021/acs.chemrev.8b00395, 2019.

Boyd, C. M., Sanchez, J., Xu, L., Eugene, A. J., Nah, T., Tuet, W. Y., Guzman, M. I., and Ng, N. L.: Secondary organic aerosol formation from the β-pinene+NO_3 system: effect of humidity and peroxy radical fate, Atmos. Chem. Phys., 15, 7497-7522, https://doi.org/10.5194/acp-15-7497-2015, 2015.

Brown, S. S. and Stutz, J.: Nighttime radical observations and chemistry, Chem. Soc. Rev., 41, https://doi.org/10.1039/c2cs35181a, 2012.

Claflin, M. S., Krechmer, J. E., Hu, W., Jimenez, J. L., and Ziemann, P. J.: Functional group composition

of secondary organic aerosol formed from ozonolysis of α-pinene under high VOC and autoxidation conditions, ACS Earth Space Chem., 2, 1196-1210, https://doi.org/10.1021/acsearthspacechem.8b00117, 2018.

Daumit, K. E., Kessler, S. H., and Kroll, J. H.: Average chemical properties and potential formation pathways of highly oxidized organic aerosol, Faraday Discuss., 165, https://doi.org/10.1039/c3fd00045a, 2013.

Donahue, N. M., Epstein, S. A., Pandis, S. N., and Robinson, A. L.: A two-dimensional volatility basis set: 1. organic-aerosol mixing thermodynamics, Atmos. Chem. Phys., 11, 3303-3318, https://doi.org/10.5194/acp-11-3303-2011, 2011.

Donahue, N. M., Henry, K. M., Mentel, T. F., Kiendler-Scharr, A., Spindler, C., Bohn, B., Brauers, T., Dorn, H. P., Fuchs, H., Tillmann, R., Wahner, A., Saathoff, H., Naumann, K.-H., Möhler, O., Leisner, T., Müller, L., Reinnig, M.-C., Hoffmann, T., Salo, K., Hallquist, M., Frosch, M., Bilde, M., Tritscher, T., Barmet, P., Praplan, A. P., DeCarlo, P. F., Dommen, J., Prévôt, A. S. H., and Baltensperger, U.: Aging of biogenic secondary organic aerosol via gas-phase OH radical reactions, P. Natl. Acad. Sci. USA, 109, 13503-13508, https://doi.org/10.1073/pnas.1115186109, 2012.

Ehn, M., Thornton, J. A., Kleist, E., Sipilä, M., Junninen, H., Pullinen, I., Springer, M., Rubach, F., Tillmann, R., and Lee, B.: A large source of low-volatility secondary organic aerosol, Nature, 506, 476-479, https://doi.org/10.1038/nature13032, 2014.

Faloona, I., Tan, D., Brune, W., Hurst, J., Barket, D., Couch, T. L., Shepson, P., Apel, E., Riemer, D., Thornberry, T., Carroll, M. A., Sillman, S., Keeler, G. J., Sagady, J., Hooper, D., and Paterson, K.: Nighttime observations of anomalously high levels of hydroxyl radicals above a deciduous forest canopy, J. Geophys. Res.-Atmos., 106, 24315-24333, https://doi.org/10.1029/2000JD900691, 2001.

Fry, J. L., Draper, D. C., Barsanti, K. C., Smith, J. N., Ortega, J., Winkler, P. M., Lawler, M. J., Brown, S. S., Edwards, P. M., Cohen, R. C., and Lee, L.: Secondary organic aerosol formation and organic nitrate yield from NO_3 oxidation of biogenic hydrocarbons, Environ. Sci. Technol., 48, 11944-11953, https://doi.org/10.1021/es502204x, 2014.

Geyer, A., Bächmann, K., Hofzumahaus, A., Holland, F., Konrad, S., Klüpfel, T., Pätz, H. W., Perner, D., Mihelcic, D., Schäfer, H. J., Volz-Thomas, A., and Platt, U.: Nighttime formation of peroxy and hydroxyl radicals during the BERLIOZ campaign: Observations and modeling studies, J. Geophys. Res.-Atmos., 108, https://doi.org/10.1029/2001JD000656, 2003a.

Geyer, A., Bächmann, K., Hofzumahaus, A., Holland, F., Konrad, S., Klüpfel, T., Pätz, H. W., Perner, D., Mihelcic, D., Schäfer, H. J., Volz-Thomas, A., and Platt, U.: Nighttime formation of peroxy and hydroxyl radicals during the BERLIOZ campaign: Observations and modeling studies, J. Geophys. Res.-Atmos., 108, https://doi.org/10.1029/2001JD000656, 2003b.

Hakola, H., Hellén, H., Hemmilä, M., Rinne, J., and Kulmala, M.: In situ measurements of volatile organic compounds in a boreal forest, Atmos. Chem. Phys., 12, 11665-11678, https://doi.org/10.5194/acp-12-11665-2012, 2012.

Hallquist, M., Wängberg, I., Ljungström, E., Barnes, I., and Becker, K. H.: Aerosol and product yields from NO_3 radical-initiated oxidation of selected monoterpenes, Environ. Sci. Technol., 33, 553-559, https://doi.org/10.1021/es980292s, 1999.

Huang, R. J., Zhang, Y., Bozzetti, C., Ho, K. F., Cao, J. J., Han, Y., Daellenbach, K. R., Slowik, J. G., Platt, S. M., Canonaco, F., Zotter, P., Wolf, R., Pieber, S. M., Bruns, E. A., Crippa, M., Ciarelli, G., Piazzalunga, A., Schwikowski, M., Abbaszade, G., Schnelle-Kreis, J., Zimmermann, R., An, Z., Szidat, S., Baltensperger, U., El Haddad, I., and Prevot, A. S.: High secondary aerosol contribution

672 to particulate pollution during haze events in China, Nature, 514, 218-222, 10.1038/nature13774,
673 2014.
674 Huang, W., Saathoff, H., Shen, X., Ramisetty, R., Leisner, T., and Mohr, C.: Chemical characterization
675 of highly functionalized organonitrates contributing to night-time organic aerosol mass loadings and
676 particle growth, Environ. Sci. Technol., 53, 1165-1174, https://doi.org/10.1021/acs.est.8b05826,
677 2019.
678 Hyttinen, N., Kupiainen-Määttä, O., Rissanen, M. P., Muuronen, M., Ehn, M., and Kurtén, T.: Modeling
679 the charging of highly oxidized cyclohexene ozonolysis products using nitrate-based chemical
680 ionization, J. Phys. Chem. A, 119, 6339-6345, https://doi.org/10.1021/acs.jpca.5b01818, 2015.
681 Inomata, S.: New particle formation promoted by OH reactions during α-pinene ozonolysis, ACS Earth
682 Space Chem., 5, 1929-1933, https://doi.org/10.1021/acsearthspacechem.1c00142, 2021.
683 Isaacman-VanWertz, G. and Aumont, B.: Impact of organic molecular structure on the estimation of
684 atmospherically relevant physicochemical parameters, Atmos. Chem. Phys., 21, 6541-6563,
685 https://doi.org/10.5194/acp-21-6541-2021, 2021.
686 Iyer, S., Rissanen, M. P., Valiev, R., Barua, S., Krechmer, J. E., Thornton, J., Ehn, M., and Kurten, T.:
687 Molecular mechanism for rapid autoxidation in alpha-pinene ozonolysis, Nat. Commun., 12, 878,
688 https://doi.org/10.1038/s41467-021-21172-w, 2021.
689 Jenkin, M., Young, J., and Rickard, A.: The MCM v3.3.1 degradation scheme for isoprene, Atmos. Chem.
690 Phys., 15, 11433-11459, https://doi.org/10.5194/acp-15-11433-2015, 2015.
691 Jokinen, T., Sipilä, M., Richters, S., Kerminen, V. M., Paasonen, P., Stratmann, F., Worsnop, D., Kulmala,
692 M., Ehn, M., and Herrmann, H.: Rapid autoxidation forms highly oxidized RO_2 radicals in the
693 atmosphere, Angew. Chem. Int. Edit., 53, 14596-14600, https://doi.org/10.1002/anie.201408566,
694 2014.
695 Junninen, H., Ehn, M., Petäjä, T., Luosujärvi, L., Kotiaho, T., Kostiainen, R., Rohner, U., Gonin, M.,
696 Fuhrer, K., and Kulmala, M.: A high-resolution mass spectrometer to measure atmospheric ion
697 composition, Atmos. Meas. Tech., 3, 1039–1053, https://doi.org/10.5194/amt-3-1039-2010, 2010.
698 Junninen, H., Hulkkonen, M., Riipinen, I., Nieminen, T., Hirsikko, A., Suni, T., Boy, M., Lee, S.-H., Vana,
699 M., Tammet, H., Kerminen, V.-M., and Kulmala, M.: Observations on nocturnal growth of
700 atmospheric clusters, Tellus B: Chemical and Physical Meteorology, 60, 365-371,
701 https://doi.org/10.1111/j.1600-0889.2008.00356.x, 2017.
702 Kenseth, C. M., Huang, Y., Zhao, R., Dalleska, N. F., Hethcox, J. C., Stoltz, B. M., and Seinfeld, J. H.:
703 Synergistic O_3 + OH oxidation pathway to extremely low-volatility dimers revealed in beta-pinene
704 secondary organic aerosol, P. Natl. Acad. Sci. USA, 115, 8301-8306,
705 https://doi.org/10.1073/pnas.1804671115, 2018.
706 Kirkby, J., Duplissy, J., Sengupta, K., Frege, C., Gordon, H., Williamson, C., Heinritzi, M., Simon, M.,
707 Yan, C., Almeida, J., Tröstl, J., Nieminen, T., Ortega, I. K., Wagner, R., Adamov, A., Amorim, A.,
708 Bernhammer, A.-K., Bianchi, F., Breitenlechner, M., Brilke, S., Chen, X., Craven, J., Dias, A.,
709 Ehrhart, S., Flagan, R. C., Franchin, A., Fuchs, C., Guida, R., Hakala, J., Hoyle, C. R., Jokinen, T.,
710 Junninen, H., Kangasluoma, J., Kim, J., Krapf, M., Kürten, A., Laaksonen, A., Lehtipalo, K.,
711 Makhmutov, V., Mathot, S., Molteni, U., Onnela, A., Peräkylä, O., Piel, F., Petäjä, T., Praplan, A. P.,
712 Pringle, K., Rap, A., Richards, N. A. D., Riipinen, I., Rissanen, M. P., Rondo, L., Sarnela, N.,
713 Schobesberger, S., Scott, C. E., Seinfeld, J. H., Sipilä, M., Steiner, G., Stozhkov, Y., Stratmann, F.,
714 Tomé, A., Virtanen, A., Vogel, A. L., Wagner, A. C., Wagner, P. E., Weingartner, E., Wimmer, D.,
715 Winkler, P. M., Ye, P., Zhang, X., Hansel, A., Dommen, J., Donahue, N. M., Worsnop, D. R.,

Baltensperger, U., Kulmala, M., Carslaw, K. S., and Curtius, J.: Ion-induced nucleation of pure biogenic particles, Nature, 533, 521-526, https://doi.org/10.1038/nature17953, 2016.

Kristensen, K., Watne, Å. K., Hammes, J., Lutz, A., Petäjä, T., Hallquist, M., Bilde, M., and Glasius, M.: High-molecular weight dimer esters are major products in aerosols from α-pinene ozonolysis and the boreal forest, Environ. Sci. Tech. Let., 3, 280-285, https://doi.org/10.1021/acs.estlett.6b00152, 2016.

Kulmala, M., Hämeri, K., Aalto, P. P., Mäkelä, J. M., Pirjola, L., Nilsson, E. D., Buzorius, G., Rannik, Ü., Dal Maso, M., Seidl, W., Hoffman, T., Janson, R., Hansson, H. C., Viisanen, Y., Laaksonen, A., and O'Dowd, C. D.: Overview of the international project on biogenic aerosol formation in the boreal forest (BIOFOR), Tellus Series B-Chemical and Physical Meteorology, 53, 324-343, https://doi.org/10.1034/j.1600-0889.2001.530402.x, 2001.

Kurtén, T., Møller, K. H., Nguyen, T. B., Schwantes, R. H., Misztal, P. K., Su, L., Wennberg, P. O., Fry, J. L., and Kjaergaard, H. G.: Alkoxy radical bond scissions explain the anomalously low secondary organic aerosol and organonitrate yields from α-pinene + NO_3, J. Phys. Chem. L, 8, 2826-2834, https://doi.org/10.1021/acs.jpclett.7b01038, 2017.

Lee, B. H., D'Ambro, E. L., Lopez-Hilfiker, F. D., Schobesberger, S., Mohr, C., Zawadowicz, M. A., Liu, J., Shilling, J. E., Hu, W., Palm, B. B., Jimenez, J. L., Hao, L., Virtanen, A., Zhang, H., Goldstein, A. H., Pye, H. O. T., and Thornton, J. A.: Resolving ambient organic aerosol formation and aging pathways with simultaneous molecular composition and volatility observations, ACS Earth Space Chem., 4, 391-402, https://doi.org/10.1021/acsearthspacechem.9b00302, 2020.

Lee, S. H., Uin, J., Guenther, A. B., de Gouw, J. A., Yu, F., Nadykto, A. B., Herb, J., Ng, N. L., Koss, A., Brune, W. H., Baumann, K., Kanawade, V. P., Keutsch, F. N., Nenes, A., Olsen, K., Goldstein, A., and Ouyang, Q.: Isoprene suppression of new particle formation: Potential mechanisms and implications, J. Geophys. Res.-Atmos., 121, https://doi.org/10.1002/2016jd024844, 2016a.

Lee, S. H., Uin, J., Guenther, A. B., de Gouw, J. A., Yu, F. Q., Nadykto, A. B., Herb, J., Ng, N. L., Koss, A., Brune, W. H., Baumann, K., Kanawade, V. P., Keutsch, F. N., Nenes, A., Olsen, K., Goldstein, A., and Ouyang, Q.: Isoprene suppression of new particle formation: Potential mechanisms and implications, J. Geophys. Res.-Atmos., 121, 14621-14635, https://doi.org/10.1002/2016jd024844, 2016b.

Li, D., Huang, W., Wang, D., Wang, M., Thornton, J. A., Caudillo, L., Rörup, B., Marten, R., Scholz, W., Finkenzeller, H., Marie, G., Baltensperger, U., Bell, D. M., Brasseur, Z., Curtius, J., Dada, L., Duplissy, J., Gong, X., Hansel, A., He, X.-C., Hofbauer, V., Junninen, H., Krechmer, J. E., Kürten, A., Lamkaddam, H., Lehtipalo, K., Lopez, B., Ma, Y., Mahfouz, N. G. A., Manninen, H. E., Mentler, B., Perrier, S., Petäjä, T., Pfeifer, J., Philippov, M., Schervish, M., Schobesberger, S., Shen, J., Surdu, M., Tomaz, S., Volkamer, R., Wang, X., Weber, S. K., Welti, A., Worsnop, D. R., Wu, Y., Yan, C., Zauner-Wieczorek, M., Kulmala, M., Kirkby, J., Donahue, N. M., George, C., El-Haddad, I., Bianchi, F., and Riva, M.: Nitrate radicals suppress biogenic new particle formation from monoterpene oxidation, Environ. Sci. Technol., 58, 1601-1614, https://doi.org/10.1021/acs.est.3c07958, 2024.

Li, X. X., Chee, S., Hao, J. M., Abbatt, J. P. D., Jiang, J. K., and Smith, J. N.: Relative humidity effect on the formation of highly oxidized molecules and new particles during monoterpene oxidation, Atmos. Chem. Phys., 19, 1555-1570, https://doi.org/10.5194/acp-19-1555-2019, 2019.

Li, Y., Pöschl, U., and Shiraiwa, M.: Molecular corridors and parameterizations of volatility in the chemical evolution of organic aerosols, Atmos. Chem. Phys., 16, 3327-3344,

https://doi.org/10.5194/acp-16-3327-2016, 2016.

Liebmann, J., Karu, E., Sobanski, N., Schuladen, J., Ehn, M., Schallhart, S., Quéléver, L., Hellen, H., Hakola, H., Hoffmann, T., Williams, J., Fischer, H., Lelieveld, J., and Crowley, J. N.: Direct measurement of NO_3 radical reactivity in a boreal forest, Atmos. Chem. Phys., 18, 3799-3815, https://doi.org/10.5194/acp-18-3799-2018, 2018.

Liu, J., D'Ambro, E. L., Lee, B. H., Schobesberger, S., Bell, D. M., Zaveri, R. A., Zelenyuk, A., Thornton, J. A., and Shilling, J. E.: Monoterpene photooxidation in a continuous-flow chamber: SOA yields and impacts of oxidants, NO(x), and VOC precursors, Environ. Sci. Technol., 56, 12066-12076, https://doi.org/10.1021/acs.est.2c02630, 2022.

Martinez, E., Cabanas, B., Aranda, A., and Martin, P.: Kinetics of the reactions of NO_3 radical with selected monoterpenes: A temperature dependence study, Environ. Sci. Technol., 32, 3730-3734, https://doi.org/10.1021/es970899t, 1998.

Mentel, T., Springer, M., Ehn, M., Kleist, E., Pullinen, I., Kurtén, T., Rissanen, M., Wahner, A., and Wildt, J.: Formation of highly oxidized multifunctional compounds: autoxidation of peroxy radicals formed in the ozonolysis of alkenes–deduced from structure–product relationships, Atmos. Chem. Phys., 15, 6745-6765, https://doi.org/10.5194/acp-15-6745-2015, 2015.

Mohr, C., Lopez-Hilfiker, F. D., Yli-Juuti, T., Heitto, A., Lutz, A., Hallquist, M., D'Ambro, E. L., Rissanen, M. P., Hao, L., Schobesberger, S., Kulmala, M., Mauldin, R. L., Makkonen, U., Sipilä, M., Petäjä, T., and Thornton, J. A.: Ambient observations of dimers from terpene oxidation in the gas phase: Implications for new particle formation and growth, Geophysical Research Letters, 44, 2958-2966, 10.1002/2017gl072718, 2017.

Molteni, U., Simon, M., Heinritzi, M., Hoyle, C. R., Bernhammer, A.-K., Bianchi, F., Breitenlechner, M., Brilke, S., Dias, A., Duplissy, J., Frege, C., Gordon, H., Heyn, C., Jokinen, T., Kürten, A., Lehtipalo, K., Makhmutov, V., Petäjä, T., Pieber, S. M., Praplan, A. P., Schobesberger, S., Steiner, G., Stozhkov, Y., Tomé, A., Tröstl, J., Wagner, A. C., Wagner, R., Williamson, C., Yan, C., Baltensperger, U., Curtius, J., Donahue, N. M., Hansel, A., Kirkby, J., Kulmala, M., Worsnop, D. R., and Dommen, J.: Formation of highly oxygenated organic molecules from α-pinene ozonolysis: chemical characteristics, mechanism, and kinetic model development, ACS Earth Space Chem., 3, 873-883, https://doi.org/10.1021/acsearthspacechem.9b00035, 2019.

Mutzel, A., Zhang, Y., Böge, O., Rodigast, M., Kolodziejczyk, A., Wang, X., and Herrmann, H.: Importance of secondary organic aerosol formation of α-pinene, limonene, and m-cresol comparing day- and nighttime radical chemistry, Atmos. Chem. Phys., 21, 8479-8498, https://doi.org/10.5194/acp-21-8479-2021, 2021.

Newland, M. J., Rickard, A. R., Sherwen, T., Evans, M. J., Vereecken, L., Muñoz, A., Ródenas, M., and Bloss, W. J.: The atmospheric impacts of monoterpene ozonolysis on global stabilised Criegee intermediate budgets and SO_2 oxidation: experiment, theory and modelling, Atmos. Chem. Phys., 18, 6095-6120, https://doi.org/10.5194/acp-18-6095-2018, 2018.

Nguyen, T. B., Crounse, J. D., Teng, A. P., St. Clair, J. M., Paulot, F., Wolfe, G. M., and Wennberg, P. O.: Rapid deposition of oxidized biogenic compounds to a temperate forest, P. Natl. Acad. Sci. USA, 112, https://doi.org/10.1073/pnas.1418702112, 2015.

Perraud, V., Bruns, E. A., Ezell, M. J., Johnson, S. N., Greaves, J., and Finlayson-Pitts*, B. J.: Identification of organic nitrates in the NO_3 radical initiated oxidation of α-pinene by atmospheric pressure chemical ionization mass spectrometry, Environ. Sci. Technol., 44, 5887–5893, https://doi.org/10.1021/es1005658, 2010.

Pye, H. O. T., Ward-Caviness, C. K., Murphy, B. N., Appel, K. W., and Seltzer, K. M.: Secondary organic aerosol association with cardiorespiratory disease mortality in the United States, Nat. Commun., 12, https://doi.org/10.1038/s41467-021-27484-1, 2021.

Schervish, M. and Donahue, N. M.: Peroxy radical chemistry and the volatility basis set, Atmos. Chem. Phys., 20, 1183-1199, https://doi.org/10.5194/acp-20-1183-2020, 2020.

Shen, H., Vereecken, L., Kang, S., Pullinen, I., Fuchs, H., Zhao, D., and Mentel, T. F.: Unexpected significance of a minor reaction pathway in daytime formation of biogenic highly oxygenated organic compounds, Sci. Adv., 8, eabp8702, https://doi.org/10.1126/sciadv.abp8702, 2022.

Shrivastava, M., Cappa, C. D., Fan, J., Goldstein, A. H., Guenther, A. B., Jimenez, J. L., Kuang, C., Laskin, A., Martin, S. T., Ng, N. L., Petaja, T., Pierce, J. R., Rasch, P. J., Roldin, P., Seinfeld, J. H., Shilling, J., Smith, J. N., Thornton, J. A., Volkamer, R., Wang, J., Worsnop, D. R., Zaveri, R. A., Zelenyuk, A., and Zhang, Q.: Recent advances in understanding secondary organic aerosol: Implications for global climate forcing, Reviews of Geophysics, 55, 509-559, 10.1002/2016rg000540, 2017.

Simon, M., Dada, L., Heinritzi, M., Scholz, W., Stolzenburg, D., Fischer, L., Wagner, A. C., Kürten, A., Rörup, B., He, X.-C., Almeida, J., Baalbaki, R., Baccarini, A., Bauer, P. S., Beck, L., Bergen, A., Bianchi, F., Bräkling, S., Brilke, S., Caudillo, L., Chen, D., Chu, B., Dias, A., Draper, D. C., Duplissy, J., El-Haddad, I., Finkenzeller, H., Frege, C., Gonzalez-Carracedo, L., Gordon, H., Granzin, M., Hakala, J., Hofbauer, V., Hoyle, C. R., Kim, C., Kong, W., Lamkaddam, H., Lee, C. P., Lehtipalo, K., Leiminger, M., Mai, H., Manninen, H. E., Marie, G., Marten, R., Mentler, B., Molteni, U., Nichman, L., Nie, W., Ojdanic, A., Onnela, A., Partoll, E., Petäjä, T., Pfeifer, J., Philippov, M., Quéléver, L. L. J., Ranjithkumar, A., Rissanen, M. P., Schallhart, S., Schobesberger, S., Schuchmann, S., Shen, J., Sipilä, M., Steiner, G., Stozhkov, Y., Tauber, C., Tham, Y. J., Tomé, A. R., Vazquez-Pufleau, M., Vogel, A. L., Wagner, R., Wang, M., Wang, D. S., Wang, Y., Weber, S. K., Wu, Y., Xiao, M., Yan, C., Ye, P., Ye, Q., Zauner-Wieczorek, M., Zhou, X., Baltensperger, U., Dommen, J., Flagan, R. C., Hansel, A., Kulmala, M., Volkamer, R., Winkler, P. M., Worsnop, D. R., Donahue, N. M., Kirkby, J., and Curtius, J.: Molecular understanding of new-particle formation from α-pinene between −50 and +25 °C, Atmos. Chem. Phys., 20, 9183-9207, https://doi.org/10.5194/acp-20-9183-2020, 2020.

Stone, D., Whalley, L. K., and Heard, D. E.: Tropospheric OH and HO_2 radicals: field measurements and model comparisons, Chem. Soc. Rev., 41, https://doi.org/10.1039/c2cs35140d, 2012.

Vereecken, L., Novelli, A., and Taraborrelli, D.: Unimolecular decay strongly limits the atmospheric impact of Criegee intermediates, Phys. Chem. Chem. Phys., 19, 31599-31612, https://doi.org/10.1039/c7cp05541b, 2017.

Wang, Y., Zhao, Y., Li, Z., Li, C., Yan, N., and Xiao, H.: Importance of hydroxyl radical chemistry in isoprene suppression of particle formation from α-pinene ozonolysis, ACS Earth Space Chem., 5, 487-499, https://doi.org/10.1021/acsearthspacechem.0c00294, 2021.

Wolfe, G. M., Marvin, M. R., Roberts, S. J., Travis, K. R., and Liao, J.: The framework for 0-D atmospheric modeling (F0AM) v3. 1, Geosci. Model Dev., 9, 3309-3319, https://doi.org/10.5194/gmd-9-3309-2016, 2016.

Xu, L., Møller, K. H., Crounse, J. D., Otkjær, R. V., Kjaergaard, H. G., and Wennberg, P. O.: Unimolecular reactions of peroxy radicals formed in the oxidation of α-pinene and β-pinene by hydroxyl radicals, J. Phys. Chem. A, 123, 1661-1674, https://doi.org/10.1021/acs.jpca.8b11726, 2019.

Zang, H., Huang, D., Zhong, J., Li, Z., Li, C., Xiao, H., and Zhao, Y.: Direct probing of acylperoxy radicals during ozonolysis of α-pinene: constraints on radical chemistry and production of highly oxygenated organic molecules, Atmos. Chem. Phys., 23, 12691-12705, https://doi.org/10.5194/acp-23-12691-2023, 2023.

Zhang, H., Yee, L. D., Lee, B. H., Curtis, M. P., Worton, D. R., Isaacman-VanWertz, G., Offenberg, J. H., Lewandowski, M., Kleindienst, T. E., Beaver, M. R., Holder, A. L., Lonneman, W. A., Docherty, K. S., Jaoui, M., Pye, H. O. T., Hu, W., Day, D. A., Campuzano-Jost, P., Jimenez, J. L., Guo, H., Weber, R. J., de Gouw, J., Koss, A. R., Edgerton, E. S., Brune, W., Mohr, C., Lopez-Hilfiker, F. D., Lutz, A., Kreisberg, N. M., Spielman, S. R., Hering, S. V., Wilson, K. R., Thornton, J. A., and Goldstein, A. H.: Monoterpenes are the largest source of summertime organic aerosol in the southeastern United States, P. Natl. Acad. Sci. USA, 115, 2038-2043, https://doi.org/10.1073/pnas.1717513115, 2018.

Zhang, X., McVay, R. C., Huang, D. D., Dalleska, N. F., Aumont, B., Flagan, R. C., and Seinfeld, J. H.: Formation and evolution of molecular products in α-pinene secondary organic aerosol, P. Natl. Acad. Sci. USA, 112, 14168-14173, https://doi.org/10.1073/pnas.1517742112, 2015.

Zhang, Y., Peräkylä, O., Yan, C., Heikkinen, L., Äijälä, M., Daellenbach, K. R., Zha, Q., Riva, M., Garmash, O., Junninen, H., Paatero, P., Worsnop, D., and Ehn, M.: Insights into atmospheric oxidation processes by performing factor analyses on subranges of mass spectra, Atmos. Chem. Phys., 20, 5945-5961, https://doi.org/10.5194/acp-20-5945-2020, 2020.

Zhao, Y., Thornton, J. A., and Pye, H. O. T.: Quantitative constraints on autoxidation and dimer formation from direct probing of monoterpene-derived peroxy radical chemistry, P. Natl. Acad. Sci. USA, 115, 12142-12147, https://doi.org/10.1073/pnas.1812147115, 2018.

Zhao, Y., Yao, M., Wang, Y., Li, Z., Wang, S., Li, C., and Xiao, H.: Acylperoxy radicals as key intermediates in the formation of dimeric compounds in α-pinene secondary organic aerosol, Environ. Sci. Technol., 56, 14249-14261, https://doi.org/10.1021/acs.est.2c02090, 2022.

Zhao, Z., Zhang, W., Alexander, T., Zhang, X., Martin, D. B. C., and Zhang, H.: Isolating alpha-pinene ozonolysis pathways reveals new insights into peroxy radical chemistry and secondary organic aerosol formation, Environ. Sci. Technol., 55, 6700-6709, https://doi.org/10.1021/acs.est.1c02107, 2021.